

# CRACK STABILITY AND TOUGHNESS CHARACTERISTICS IN BRITTLE MATERIALS<sup>1</sup>

*Yiu-Wing Mai<sup>2</sup> and Brian R. Lawn*

Institute for Materials Science and Engineering, National Bureau of Standards, Gaithersburg, Maryland 20899

## INTRODUCTION

Modern-day theories of the strength of brittle materials stem from the Griffith energy balance description of fracture processes (1). Griffith regarded a cracked body as a thermodynamic system: a crack exists in a state of equilibrium if, for a virtual incremental extension, the release of mechanical energy in the system balances the work to create the new surface area. In current "fracture mechanics" notation this critical state may be expressed as  $G_a = G_c$  or  $K_a = K_c$ , where the crack extension force  $G_a$  and stress intensity factor  $K_a$  identify with the mechanical energy term, and  $G_c$  and  $K_c$  similarly identify with the surface work term (2). From a practical standpoint this simple "crack law" has a broad appeal. By measuring the applied loads needed to cause the extension of well-defined cracks we can determine intrinsic material "resistance" or "toughness" parameters, which can then be used in design against brittle failure.

However, simple as it seems, the crack law embodied in the relations  $G_a = G_c$  and  $K_a = K_c$  is the source of much misunderstanding and improper application in the fracture testing community, particularly by those who

<sup>1</sup> The US Government has the right to retain a nonexclusive, royalty-free license in and to any copyright covering this paper.

<sup>2</sup> On leave from Department of Mechanical Engineering, University of Sydney, Sydney, New South Wales 2006, Australia.

deal with nonmetals. It is widely taken that such relations define the condition for failure. This is not so. The equilibrium law does indeed relate to crack extension, but makes no statement as to whether this extension is unstable or stable. For the idealized crack configuration originally considered by Griffith, that of an otherwise stress-free crack in a homogeneous body loaded in uniform tension, the equilibrium state is in fact *unstable*, so failure can be identified with the attainment of a critical  $G_c$  or  $K_c$ . However, as first pointed out by Barenblatt (3), there are many loading configurations in which the equilibrium crack states are *stable*, such that extension occurs only in response to a continual increase in the applied driving force. Hence, in general,  $K_a = K_c$  (or its  $G$ -term equivalent) constitutes a necessary but not sufficient condition for failure; an additional instability requirement must also be satisfied. It is possible, for instance, to conceive of loading configurations for which the equilibrium crack begins its extension in a stable mode and, after a significant increase in the applied load level, becomes unstable at a later stage of development (3, 4). Totally erroneous conclusions can be drawn concerning fracture properties if due attention is not given to these stability conditions.

There is growing evidence that crack-stabilization influences are manifest in the strength characteristics of many material types. In practice, one usually sets out to measure strengths in loading configurations that essentially reflect the idealization of Griffith, namely uniform tensile stress over the prospective crack plane, so that the time-honored critical stress notions of spontaneous failure from an initially stress-free crack (flaw) can be assumed to hold. It is becoming more and more apparent that several "internal" sources of crack driving force can exist, over and above the external applied loading, which can contribute to the net  $K$  field at the crack tip. In such cases we must reconsider the fracture mechanics requirements for failure. Several specific examples of such internal sources are discussed later in this review.

In this presentation we examine the ways in which the conventional strength descriptions need to be modified to incorporate these additional mechanical factors. There are two distinct philosophies that can be adopted here. The first relates more closely to structural design. In this philosophy we regard the internal  $K$  terms as modifying the surface work parameter  $K_c$ , so  $K_a$  remains the sole mechanical driving force on the crack system. The appeal of this approach is that one does not require a priori knowledge of the extra  $K$  terms. These extra terms are simply reflected in the measured toughness characteristics, obtained directly from the applied-load/crack-size responses of well-defined test configurations. However, the toughness now can no longer be specified as a material constant; rather, it becomes

some empirical function of the crack geometry. This description closely parallels the familiar “*R*-curve” function in metals, in which plane-stress shear-lip formation increases resistance to propagation as the crack extends from its initial size (5).

The second philosophy asserts that the internal  $K$  terms are more properly regarded as augmenting the applied stress intensity factor  $K_a$ . The toughness term  $K_c$  can now indeed be retained as a material invariant. (However, in view of much past confusion over the meaning of this toughness term, we propose its replacement by an alternative symbol,  $T$ .) This approach is especially attractive to the materials scientist, who ultimately seeks to relate the laws of crack growth to fundamental “constants” of solids (if possible, at the atomic level). The fundamental information comes only at a price: one first needs to learn how to account for all the internal contributions to the net  $K$  field. Our choice of this second route boils down to how much more we value physical understanding over practical expediency.

Accordingly, we begin our analysis by laying down the requirements for fracture instability in general terms, using the Griffith energy balance as the key starting point. These requirements are most conveniently expressed in stress intensity factor notation, so that the internal driving force terms may be simply incorporated by linear superposition of  $K$  fields (2). We then present some case studies that show strong contributions to the fracture properties from internal sources. These case studies embrace two crack geometries, precracked beam and indentation flaw, and a wide range of brittle material types, from simple silicate glasses to complex composites. The evidence shows that one must be extremely careful when interrelating strength and toughness characteristics. The implications of these results in connection with the validity of conventional crack laws are also briefly considered.

## GENERAL DESCRIPTION OF CRACK STABILITY CONDITIONS

### *Theoretical Formulation*

The general conditions for crack stability may be formulated directly from the Griffith energy balance concept (1, 4). The total energy  $U$  of a crack system is made up of two components, the mechanical energy,  $U_m$  (elastic strain energy plus potential energy of loading), and the surface work,  $U_s$ . A state of equilibrium is reached when the energy has a stationary value with respect to any virtual change in the crack area  $C$ , i.e.

$$dU/dC = dU_m/dC + dU_s/dC = 0.$$

1.

It is convenient to define the quantities

$$G = -dU_m/dC \quad \text{and} \quad 2a.$$

$$-R = -dU_s/dC \quad 2b.$$

so that Equation 1 reduces to the familiar form

$$G = G_c = R, \quad 3.$$

where subscript *c* denotes an equilibrium configuration. *G* is Irwin's mechanical energy release rate (2); it characterizes the forces that drive the crack. *R* characterizes the resistance forces associated with the surface formation processes. Of these two quantities, only *R* relates directly to intrinsic properties of the material. Of course, for ideally brittle solids *R* is equivalent to the surface free energy,  $2\gamma_s$ .

Equation 3 tells us when a crack is on the verge of extension, but it is not a sufficient condition for failure. For failure, the equilibrium has to be unstable. We indicated in our introduction that not all equilibrium crack systems are of the unstable kind; the crack extension may occur in a stable fashion with each increment in applied load. To determine the nature of the equilibrium we have to consider the second derivative of energy,  $d^2U/dC^2$ . The system is unstable or stable depending on whether this second derivative is less than or greater than zero. In terms of Equations 1 and 2, we obtain

$$dG/dC > dR/dC \quad (\text{unstable}) \quad 4a.$$

$$dG/dC < dR/dC \quad (\text{stable}).^3 \quad 4b.$$

In the event of *R* independent of *C* the right side of Equation 4 is zero; then (and only then) the stability is determined exclusively by whether *G* is an increasing or decreasing function of *C*.

Equation 4 may be equivalently expressed in stress intensity factor notation. Using connecting equations between *K* and *G* from linear elastic fracture mechanics (2, 4, 5), we write

$$K = (GE)^{1/2} \quad \text{and} \quad 5a.$$

$$T = (RE)^{1/2}, \quad 5b.$$

where *E* is Young's modulus. (Strictly, these relations are for plane stress; *E* should be replaced by  $E/(1-\nu^2)$  for plane strain, where  $\nu$  is Poisson's ratio.) *T* is interpreted as a material toughness parameter. The equilibrium

<sup>3</sup> Actually, there is a third equilibrium state, "neutral," determined by an equality condition in Equation 4.

relation (Equation 3) may now be expressed as

$$K = K_c = T. \quad 6.$$

Likewise, the stability relations of Equation 4 for such equilibrium states transform to

$$dK/dC > dT/dC \quad (\text{unstable}) \quad 7a.$$

$$dK/dC < dT/dC \quad (\text{stable}). \quad 7b.$$

Again, if  $T$  turns out to be independent of  $C$  the stability is determined exclusively by the functional dependence of  $K(C)$ .

The main advantage of the stress intensity factor notation here is that the  $K$  terms *for a given mode of fracture* (hereinafter assumed always to be opening Mode I) are additive quantities, whereas the  $G$  terms are not (2, 4, 5). Thus, if there are internal contributions,  $K_i$ , to the crack driving force, we may superpose these linearly onto the *true* applied loading contribution,  $K_a$ , to get (6)

$$K = K_a + \sum_i K_i. \quad 8.$$

$K$  is the effective driving force felt at the crack tip. The  $K_i$  terms in Equation 8 can be viewed as having a shielding or antishielding influence on the transmission of externally applied stresses to the crack tip, depending on whether the signs are negative or positive. It is generally possible to express the internal terms as an integral over tractions  $\sigma_i(X)$  at the crack interface,

$$K_i = \int_0^c g(C, X) \sigma_i(X) dX, \quad 9.$$

where  $X$  is an area coordinate measured from the origin in the crack plane and  $g(C, X)$  is an appropriate Green's function. Inserting  $K$  in Equation 8 into Equation 6 gives the modified equilibrium relation

$$K(C) = T_0, \quad 10.$$

where the subscript zero on the  $T$  term denotes a *material-invariant* toughness (i.e. the toughness if the  $K_i$  terms were entirely absent). The conditions for instability or stability in Equation 7 translate to

$$dK/dC = dK_a/dC + d\left(\sum_i K_i\right)/dC \gtrless 0. \quad 11.$$

We can choose to associate the internal factors with the toughness term rather than with the mechanical driving force term (see the introduction).

Accordingly, we define the effective toughness as

$$T = T_0 - \sum_i K_i, \quad 12.$$

in analogy to Equation 8. The modified equilibrium relation retains the same simple form as Equation 10,

$$K_a(C) = T(C), \quad 13.$$

except that now  $T$  cannot be regarded as a material invariant (although the *function*  $T(C)$  might still be a material property; see the case studies, below). The instability/stability conditions of Equation 7 now become

$$dK_a/dC \geq dT/dC. \quad 14.$$

Equations 12–14 provide the basis for the  $R$ -curve (or, more appropriately, the  $T$ -curve) description.

### *Experimental Procedures*

From the standpoint of the experimentalist, the crack stability and toughness characteristics should be determinable from the responses of well-defined fracture configurations. One usually seeks to design fracture specimens of simple geometry so that the essential fracture mechanics terms above, most notably  $K_a$ , can be specified as explicit functions of some characteristic linear crack coordinate,  $c$ . This linear coordinate may be a crack length (straight-fronted crack) or crack radius (penny crack), etc. Clearly, the linear coordinate  $c$  is interchangeable with the areal coordinate  $C$  in the previous stability relations, Equations 7, 11, and 14. Thus, armed with a means of monitoring the functional dependence  $K_a(c)$ , we may generate the  $T$ -curve function  $T(c)$  in Equation 13 by following the crack growth through its stable equilibrium states to the point of instability.

With this information, we may then quantify the internal contributions to the net crack driving force. This may be done empirically by using Equation 12 to evaluate the  $K_i$  terms. Note that this approach is contingent on our ability to determine the intrinsic baseline toughness,  $T_0$ , from the experimental data. Alternatively, and preferably, we might hope to evaluate the  $K_i$  terms from first principles, thereby allowing for a direct determination of  $K(c)$  in Equation 8 from the raw experimental data. Equation 10 then becomes the appropriate equilibrium equation for characterizing the toughness. Of course, this latter alternative requires that we have a priori knowledge of the mechanisms actually responsible for the  $K_i$  contributions.

There are two important points concerning the design of test configurations that should be brought out here. The first relates to the “rigidity”

of the loading system (7). This factor can be strongly reflected in the quantity  $dK_a/dc$  which appears in Equations 11 and 14. In the extremes of "hard" (constant displacement  $\delta$ ) and "soft" (constant force  $P$ ) loading devices the differential reduces to the partial forms,  $(\partial K_a/\partial c)_\delta$  and  $(\partial K_a/\partial c)_P$ , which can have widely different dependences on  $c$ . Generally, the more rigid the loading device the greater the stability of the crack system. The second point relates to the specimen geometry. It is implicit in most analyses that the crack size should be small compared to specimen dimensions, but large compared to the dimensions over which internal forces act. Violation of these conditions can seriously complicate the analytical forms of the  $K_a(c)$  and  $K_i(c)$  functions, thereby yielding variations in the apparent toughness characteristics from specimen to specimen. In cases like these special care must be exercised in interpreting the role of the  $K_i$  terms, i.e. whether we associate these terms with  $K_a$  (Equation 8) or  $T_0$  (Equation 12).

To illustrate the principles outlined above we devote the next two sections to specific case studies. We focus on two kinds of fracture configurations, precracked beam (double cantilever, single-edge notched bend) and indentation flaw. The precracked beam case allows relatively simple, direct crack length measurements. The indentation flaw system avoids the need for any direct crack measurements by reformulating the critical strength relations in terms of a more accessible test variable, indentation load. Our choice of just two configuration types is not restrictive; the effects we describe are evident in all test geometries (notwithstanding the complicating factors referred to in the previous paragraph).

## PRECRACKED BEAM SYSTEMS: CASE STUDIES

Conventional fracture toughness testing employs specimen geometries such as the double-cantilever beam (DCB) and single-edge notched bend (SENB) systems (8). These specimens are particularly suited to direct observation of crack growth during applied loading. Generally, the growth is measured as the position  $\Delta c$  from the tip of a linear starter crack or notch of length  $c_0$ . This starter crack is usually cut or sawn into the specimen so that it retains no "memory" of the structure that contains it. Measurements of crack growth can then be used to construct the  $T$ -curve.

### *DCB Study on Polycrystalline Alumina*

In this subsection we look at some results obtained on a polycrystalline alumina ceramic using the DCB test geometry. This will demonstrate that the  $T$ -curve phenomenology extends to the "simplest" of brittle materials. Alumina is often used as a "model" ceramic material by the fracture testing

community because it can be readily obtained in a monophase form with well-characterized grain structures. It is often supposed to be free of the microstructural complications that characterize other, more practical structural materials (discussed in later sections). Nevertheless, in the results described here, obtained by Swain (9) on the same alumina material used in an earlier, notched beam study by Knehans & Steinbrech (10), it becomes evident that even near-ideal microstructures can exhibit long-range effects.

In the DCB test one usually monitors the crack extension  $\Delta c$  from a starter crack  $c_0$  as a function of either the applied load,  $P$ , at the beam mouth or the displacement,  $\delta$ , at that point. Then the applied stress intensity factor can be evaluated in terms of the total crack length,  $c = c_0 + \Delta c$ ,

$$K_a = \alpha_1 P c \quad (\text{constant load}) \text{ and} \quad 15a.$$

$$K_a = \alpha_2 \delta / c^2 \quad (\text{constant displacement}), \quad 15b.$$

where  $\alpha_1$  and  $\alpha_2$  can be expressed in terms of specimen dimensions such as width, thickness, groove size (and even crack size) (8). Over its range of equilibrium growth, the crack configuration allows us to trace out the function  $T(c)$  in Equation 13.

Figure 1a shows Swain's alumina data, which were obtained at constant displacement. The effective toughness  $T(c)$ , shown as a solid curve, almost doubles over a crack extension of some 10 mm. The inverted dashed curves are representations of  $K_a(c)$  in Equation 15b at different values of  $\delta$ . Here the condition  $(\partial K_a / \partial c)_\delta < dT/dc$  is always satisfied, so the crack extension is never unstable, i.e. the crack grows continuously with increasing  $\delta$ . In this mode, therefore, we can trace out the entire  $T$ -curve, from the initial value  $T_0$  to the ultimate saturation level at large  $\Delta c$ .

A different response is observed in tests at constant load. To show this, we plot Equation 15a as dashed straight lines through the origin for different values of  $P$  in Figure 1a. At low load the crack remains stationary. The crack does not extend until the load line intersects the point  $(c_0, T_0)$ . Stable growth then ensues until a condition of tangency is achieved at  $M$ , which corresponds to the instability requirement  $(\partial K_a / \partial c)_P \geq dT/dc$ . This is the point of failure. Note the substantial extent of stable growth,  $(\Delta c)_M \approx 3$  mm. Beyond this point, however, the instability precludes further  $T$ -curve measurements, i.e. the curve cannot be determined beyond  $M$  at constant load.

We may now ask whether the  $T$ -curve in Figure 1a is representative of a material property. The first indication that it may not be is that the position of the curve clearly depends on the starter crack size. We note that the instability point at  $M$  for constant load conditions is a function

of  $c_0$ . Hence  $T(c)$  depends on crack history. We might argue that the effective crack origin should be taken at  $c_0$ , in which case  $T(\Delta c)$  is more likely to be the material property. However, Knehans & Steinbrech (10), in their notched beam experiments, have demonstrated that even this function is crack-history dependent. (Indeed, the results obtained by those authors are quite different from Swain's DCB data, although the source material was the same.) We must conclude that the  $T$ -curve is not invariant for a given material, but tends to vary with specimen geometry.

We believe that the root of this variability lies in the fact that the  $T$ -curve

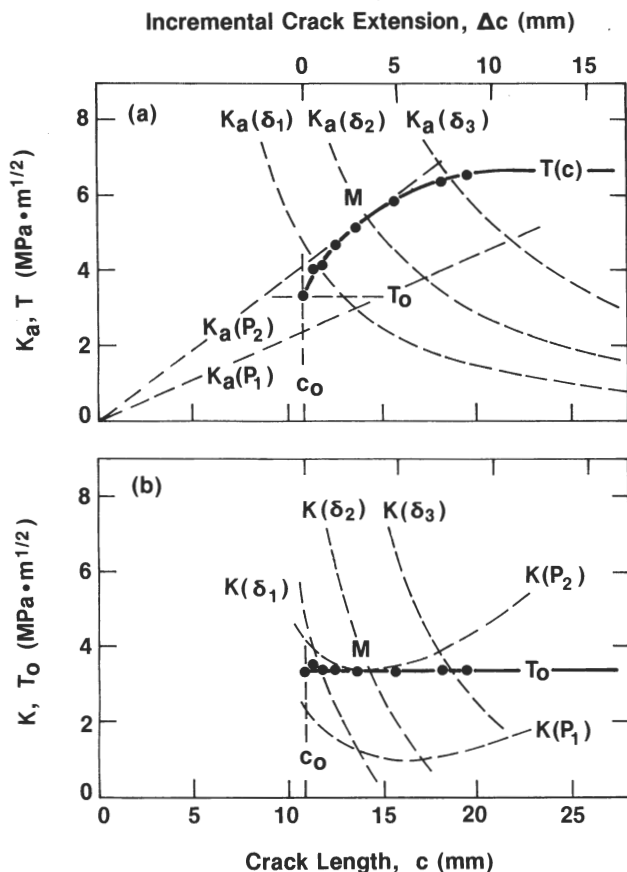


Figure 1 Crack toughness data for a polycrystalline alumina (nominally pure, grain size 16  $\mu\text{m}$ ), obtained on a DCB specimen: (a) direct  $T$ -curve construction, with  $K_I = K_\mu$  included in the toughness curve; (b) replot of the same data, with  $K_\mu$  subtracted out from the toughness curve. (Data courtesy of M. V. Swain.)

contains the  $K_i$  contributions, which may themselves include geometrical factors. We should associate these  $K_i$  contributions with the applied term  $K_a$ , as in Equation 8, so that  $T_0$  in Equation 10 can be isolated as the true material invariant. For the polycrystalline alumina examined here, the cracking is found to be predominantly intergranular (9), so we must consider an intrinsic grain boundary toughness term. Measuring  $T_0$  as the base of the  $T$ -curve in Figure 1a, we can use Equation 12 to evaluate  $\Sigma K_i$  at each data point and thence generate appropriate  $K(c)$  functions from Equation 8. Figure 1b shows the results of Figure 1a replotted in accordance with this set of transformations. The graphical constructions for describing the crack response are analogous to those in Figure 1a, except of course that Equations 10 and 11 now define the equilibrium and stability states. The major advantage of the alternative plotting procedure is that the toughness characteristic no longer contains any elements of crack-history or geometry dependence; the emphasis shifts to the fracture mechanics analyst, to determine how the complicating elements may be incorporated directly into the  $K(c)$  function.

What is it about polycrystalline alumina that gives rise to noninvariant toughness properties? What material parameters determine the  $K_i$  terms, and how do geometrical effects contribute to these terms? It appears that the answers to such questions are most likely to be found at the newly formed crack interface *behind* the advancing tip (11). It has been observed that cracks are "bridged" by grain-localized ligaments that exert restraining forces on the system. These ligaments can remain active several millimeters behind the crack tip, much as in fiber-reinforced composites (see section on fiber-reinforced cement, below). As the crack extends, the number of restraining elements increases, thereby causing the toughening. This toughening (hence the  $T$ -curve) only reaches a plateau when the grain ligaments begin to rupture. The appropriate internal stress intensity factor,  $K_\mu$ , associated with the microstructure can be calculated from Equation 9, where  $\sigma_i(x)$  is the distribution (assumed to be continuous) of closure stresses. Note that the integral is over the active crack length, i.e. from  $c_0$  to  $c$ , which accounts for the geometry dependence. It can be shown that Equation 9 transforms to

$$K_\mu(c) = -(E/T_0) \int_0^{u_0} \sigma_i(u) du, \quad 16.$$

approximately, where  $E$  is Young's modulus and  $u_0 = u(x = c_0; c)$  is the crack opening displacement at the point along the interface where bridging is first encountered (in this case at the starter crack,  $c_0$ ) (11). The material dependence therefore involves  $E$ ,  $T_0$ , and the work to rupture the ligaments.

Details of the evaluation of Equation 16 (which currently has to be carried out numerically) are given elsewhere (12). Suffice it to say that the solid curve in Figure 1a has been fitted in accordance with such an evaluation.

### *SENB Study on a Phase Transforming Zirconia*

Zirconia ceramics are now being extensively studied for their great potential as structural materials (13). Their high toughnesses are contingent on the ability of the ceramics processor to stabilize the zirconia structure (e.g. by the use of favorable additives) so that the matrix material contains metastable tetragonal phase particles. The intense stress field of an advancing crack triggers a martensitic transformation in these particles, to a more dilate monoclinic phase. The net result is an effective closure force on the crack. Since the matrix zirconia itself has relatively low toughness, we have the ingredients of strong *T*-curve behavior. We use data collected by Swain & Hannink (14) on an SENB specimen to illustrate this point.

The SENB specimen, like its DCB counterpart, is prepared with a starter crack,  $c_0$ . The precracked beam is then loaded in flexure, with load  $P$  or load-point displacement  $\delta$ . The applied stress intensity factor is given by (8)

$$K_a = \beta_1 P c^{1/2} \quad (\text{constant load}) \quad \text{and} \quad 17a.$$

$$K_a = \beta_2 \delta c^{1/2} \quad (\text{constant displacement}), \quad 17b.$$

where  $\beta_1$  and  $\beta_2$  are functions of the specimen dimensions. In particular, the  $\beta$  functions are strongly dependent on the ratio of crack size to specimen width,  $c/w$ . Indeed, the difference in crack stability at constant load and constant displacement is entirely accounted for by the difference in  $c/w$  dependence between  $\beta_1$  and  $\beta_2$ . Given suitable calibrations for these factors, we can map out the equilibrium *T*-curve as in the previous example.

Such a curve has been plotted for the Swain & Hannink zirconia data in Figure 2. The data show the same trends as in Figure 1, except that the degree of toughening is greater and the range of crack extension to saturation is shorter. As before, the upper plot (solid curve) represents the as-measured *T*-curve, and the lower represents the equivalent curve with the  $K_i$  terms subtracted out. In each case we include appropriate loading lines (dashed curves) at both constant load and displacement. Again, the constant load configuration has an instability at  $M$ , preceded by stable growth of about  $(\Delta c)_M = 100 \mu\text{m}$ , whereas the constant displacement configuration is always stable.

A physical model of the transformation toughening mechanics has been developed by McMeeking & Evans (15). They derive an expression for the

internal, transformation-associated stress intensity factor of the form

$$K_t(c) = -Ee^t v_f \omega^{1/2} \Phi(\Delta c / \omega), \quad 18.$$

where  $E$  is Young's modulus,  $e^t$  the unconstrained dilatational strain of a tetragonal-monoclinic transformation,  $v_f$  is the volume fraction of the (initially) tetragonal phase,  $\nu$  is Poisson's ratio, and  $\omega$  is the width of the transformed zone at the wake of the fully extended crack. A tabulation of the function  $\Phi(\Delta c / \omega)$  by McMeeking & Evans (15) has been used to fit the curve to the data in Figure 2a, using the matrix toughness  $T_0$  as the reference baseline in Equation 12.

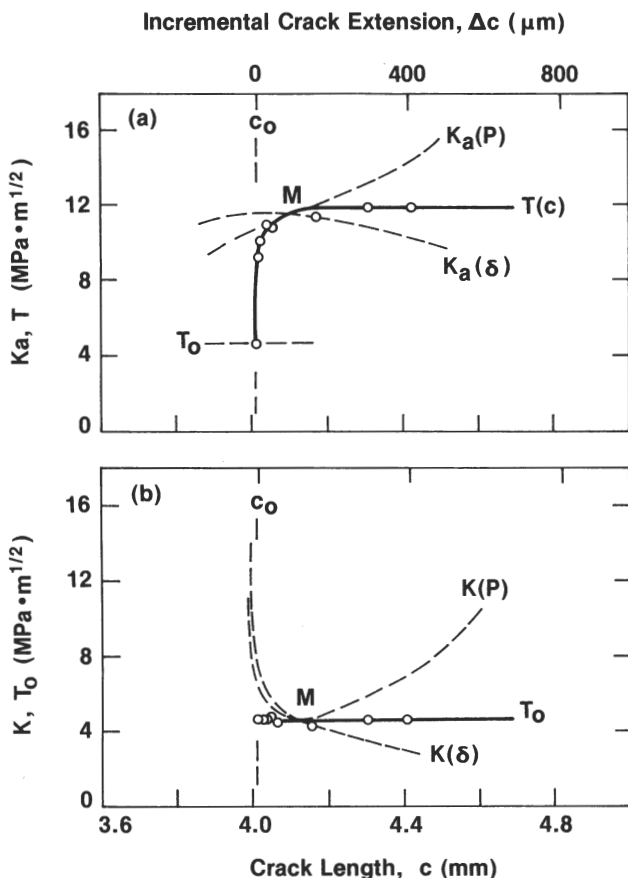


Figure 2 SENB crack toughness data for a zirconia ceramic (magnesia stabilized): (a) direct  $T$ -curve construction; (b) replot, with  $K_i = K_t$  subtracted out from  $T(c)$ . (Data from Reference 14.)

Some more recent experiments on zirconia materials with particularly high toughening have revealed zone sizes that are not insignificant in comparison with specimen dimensions (16, 17). Thus, as with alumina, geometrical effects are felt in the  $T$ -curve. Again, it is only  $T_0$ , not  $T(c)$ , that can truly be regarded as material invariant.

### *SENB Study on a Fiber-Reinforced Cement Composite*

Let us now look at the toughness properties of an asbestos fiber cement (18). Here we focus more closely on specimen size effects, by studying results from SENB beams of different thickness.<sup>4</sup> Fiber-reinforced materials are ideal for this purpose because the interfacial bridging restraint exerted by the fibers on the crack growth is very long range. The starter crack is cut into the beam so there is no bridging at  $c \leq c_0$ , in which case the toughness  $T_0$  at the first incremental extension is precisely that of the cement matrix. The full  $T$ -curve can then be generated in the way described in the previous section, using the displacement-controlled solution in Equation 17 (18).

The resulting data are plotted in Figure 3 for three beam thicknesses,  $w$ . It is immediately clear that there is a strong size effect, despite the large thicknesses used (25–150 mm). Again, we can subtract out the internal  $K_i$  terms from the  $T$ -curve in Figure 3a and generate a horizontal line  $T_0 = \text{constant}$  in Figure 3b. Theoretically, analysis of these results becomes relatively complex, for not only are the  $K_a$  terms in Equation 17 strongly dependent on  $c/w$ , but so also are the  $K_i$  terms. A detailed calculation based on Equation 9 gives the stress intensity associated with fiber reinforcement as (19)

$$K_f(c) = -\psi \int_{c_0}^c c^{-1/2} F(c/w, c_0/w) \sigma_i(x) dx, \quad 19.$$

where  $\psi$  is a numerical constant,  $F(c/w, c_0/w)$  is a dimensionless function obtainable from stress intensity factor handbooks (20), and  $\sigma_i(x)$  can be measured empirically in tensile tests on specimens with completely developed matrix cracks. Such a calculation has been used to fit the curves (solid lines) to the data in Figure 3a and to generate the loading lines (dashed) in Figure 3b. Note that the latter are all for a single fixed displacement  $\delta$ , so the relative shifts are due entirely to the influence of specimen size on the effective driving force felt at the crack tip.

Thus, as with the other cases we have considered so far, it is the intrinsic

<sup>4</sup> By "thickness" we mean the beam dimension measured in the direction of crack propagation.

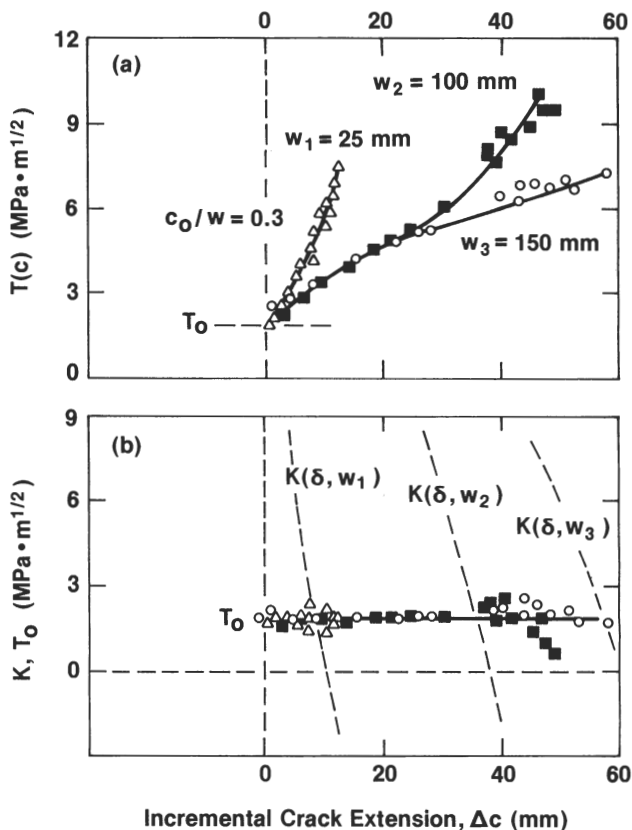


Figure 3 SENB crack toughness data for an asbestos-reinforced cement, showing specimen thickness effects, for fixed  $c_0/w$ : (a) direct  $T$ -curve plot; (b) same data with  $K_i = K_r$  subtracted out from  $T(c)$ . (Data from Reference 18.)

“matrix” toughness  $T_0$  that remains the true material invariant for equilibrium fracture. The role of the internal sources that give rise to the apparent increase in this base toughness level as the crack extends (even though these sources may themselves involve material properties) is most appropriately evaluated in terms of the shielding concepts embodied in the Greens function formalism of Equation 9.

## INDENTATION FLAW SYSTEMS: CASE STUDIES

One of the most versatile techniques for determining the fracture properties of highly brittle materials is that of indentation (21, 22). A Vickers indenter is used to introduce a controlled flaw into the surface of a test specimen.

Unlike the starter crack in the previous specimen types, this flaw “remembers” fully the material structure in which it evolved. The specimen is then broken in flexure. Apart from affording a means for quantifying the toughness, via the strength/indentation-load relation, the technique provides much new insight into the stability characteristics of natural flaw types.

### *Residual-Contact Stresses: A Study on Glass*

A crucial feature of the indentation flaw system is the role that residual-contact tensile driving forces play in the fracture evolution (23–25). This influence is felt at all stages: *during* contact, in the initiation and development of radial cracks (particularly as the indenter is being unloaded) and *after* contact, when (most notably in the presence of water vapor) cracks can continue to grow. Most importantly, the residual fields persist through subsequent strength testing in a way that stabilizes the cracks. If we are to use the indentation-strength method for evaluating toughness properties it is imperative that we learn how to accommodate this additional factor in the fracture mechanics.

One of the great advantages of the indentation flaw system is that the failure origin is predetermined, so we can set up a microscope to monitor the crack size  $c$  as a function of the applied stress  $\sigma_a$ . Data from such observations by Marshall and coworkers (24) are shown in Figure 4a. These data are for tests on soda lime glass in an inert environment (i.e. equilibrium conditions) at two Vickers indentation loads. There is substantial stable crack growth prior to failure at the maximum point  $M$  of each curve (24), contrary to the notion of spontaneous instability usually associated with the classical Griffith-like flaw.

If we now replot the data in accordance with Equation 13 we see that the response corresponds, in effect, to  $T$ -curve behavior. To obtain such a plot we use the standard expression for the applied stress intensity factor in a strength test,

$$K_a = \psi \sigma_a c^{1/2} \quad (\text{constant stress}), \quad 20.$$

where  $\psi$  is a numerical constant. (We assume here that the flaw size is always sufficiently small that beam thickness effects may be ignored.) The resultant  $T$ -curve is shown in Figure 4b. The instability points  $M$  correspond to the usual point of tangency. (Note again that because of this instability we are unable to obtain data beyond  $M$ .) The data for the two indentation loads fall on separate  $T$ -curves, although the critical value of  $T(c)$  at instability is load independent.

To account for the results in Figure 4b, in particular the dependence of the  $T$ -curve on load, we need to incorporate an internal stress intensity

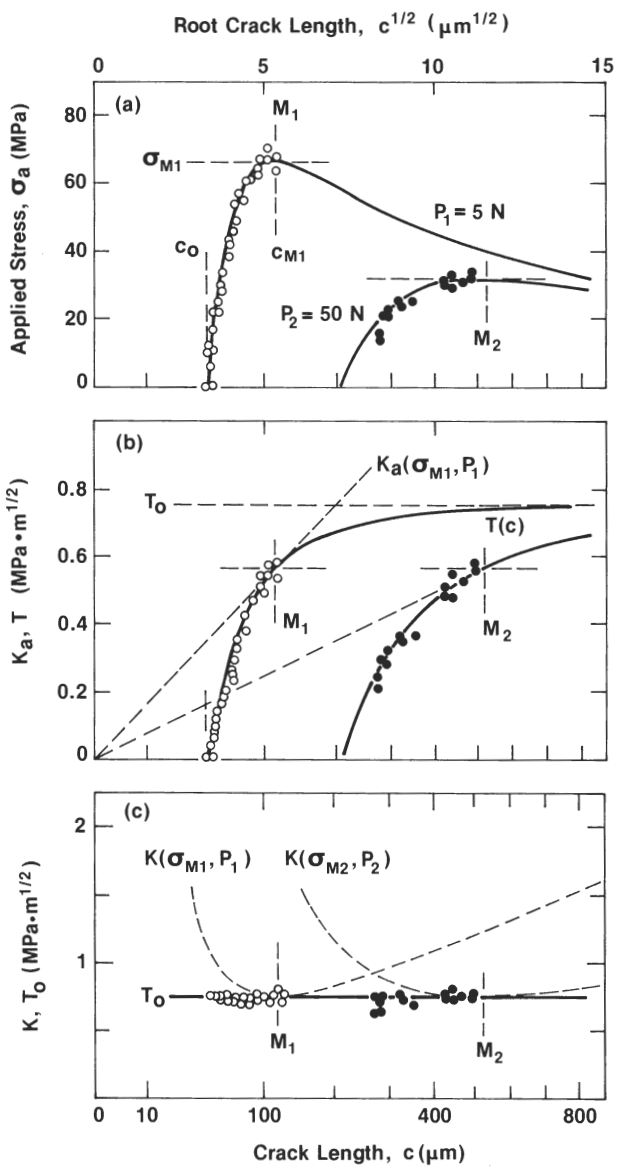


Figure 4 Crack growth data for Vickers indentation flaws in soda lime glass bend specimens : (a) applied stress versus crack size, at two indentation loads ; (b) equivalent  $T$ -curve construction ; (c) replot, with  $K_i = K_r$  subtracted out from  $T(c)$ . (Data from Reference 24 and courtesy of D. B. Marshall.)

factor associated with the tensile residual contact field. This contribution can be determined as a limiting case of Equation 9, appropriate to a center-loaded penny-shaped radial crack (23, 25, 26):

$$K_r(c) = \chi P / c^{3/2}, \quad 21.$$

where  $\chi$  is a dimensionless elastic-plastic constraint factor. In Figures 4a and b the solid curves are appropriate data fits, where we have treated  $T_0$  and  $\chi$  as adjustable parameters in the equilibrium relation  $K_a = T_0 - K_r = T$ . Thus it is through  $K_r$  that  $P$  enters as a variable. The instability configurations at  $M$  may now be determined explicitly by setting  $(\partial K_a / \partial c)_{\sigma_a} = -dK_r/dc$  (Equation 11), yielding

$$K_M = \psi \sigma_M c_M^{1/2} = 3T_0/4, \quad 22.$$

which is *independent* of load (or, equivalently, of the initial crack size). The locus of the instability points  $M$  in Figure 4b, notwithstanding the history factor in the  $T$ -curves themselves, provides us with a measure of the intrinsic material toughness,  $T_0$ . Special note may be made here of the fact that the internal term  $K_r$  is positive and decreasing with respect to crack extension, such that the  $T$ -curve tends to  $T_0$  at large  $\Delta c$ . This is in contrast to the precracked examples discussed earlier, in which the  $K_i$  terms were all negative and increasing with crack extension, such that the baseline level  $T(c) = T_0$  was obtained at zero  $\Delta c$ .

It is interesting that the inverse square root relationship between critical stress and flaw size in Equation 22 is the same as that for classical Griffith-like flaws (i.e. for  $K_r = 0$  in the equilibrium relation). Effectively, the residual stress simply reduces the strength by 3/4 in Equation 22. Therefore, measurement of the strength/crack-size dependence alone is not sufficient to reveal the nature of the equilibrium conditions that precede failure. It is therefore possible that important departures from ideal Griffith instability may pass entirely unnoticed in some crack observation procedures, e.g. in postfailure fractographic examination of flaw origins.

Our conclusion that  $T(c)$  is not material intrinsic, whereas  $T_0$  is, suggests that  $K_r$  should be coupled as an antishielding term with the applied driving force. This conviction is reinforced when we look more closely at the parameters involved in  $K_r$ . Unlike our previous  $K_i$  terms (in the section on precracked beam systems), there are no elements of material dependence in Equation 21 [notwithstanding a minor dependence of  $\chi$  on modulus and hardness (25)] that might be associated with an intrinsic toughness characteristic. Thus, in the spirit of Equation 10, we can transform the graphical representation in Figure 4b to that of Figure 4c by making use of our "calibrated" values of  $T_0$  and  $\chi$ , as in Figures 1–3. The elements of crack history (as reflected here in the value of  $P$ ) are now bound up

exclusively in the loading lines,  $K(c)$ , isolating  $T_0$  as the true toughness parameter.

There is something very useful that we can draw from our analysis of the indentation problem at this stage. Clearly, we must observe the crack growth directly during stressing to confirm the crack-size dependence of the  $K_r$  term in Equation 21. However, once this dependence has been established there is little to be gained by repeating the observations in subsequent failure test runs. In principle, it should suffice to monitor the system at the critical points  $M$  only, for, as seen in Equation 22, these points uniquely determine the material toughness parameter. Indeed, one can eliminate the necessity for *any* further measurements of crack size because the instability condition,  $dK/dc = (\partial K_a/\partial c)_{\sigma_a} + dK_r/dc = 0$ , can be used in conjunction with the equilibrium relation,  $K = K_a + K_r = T_0$ , to obtain

$$\sigma_M P^{1/3} = 3T_0^{4/3}/4^{4/3}\psi\chi^{1/3} = \text{constant}, \quad 23.$$

thus eliminating  $c$  as a variable. (Equation 23 is equivalent to Equation 22, but  $P$  replaces  $c_M$  as a measure of flaw severity.) This is a distinct advantage in studying ceramics in which crack observations are not always practical, owing to poor optical reflectivity, ill-developed radial crack patterns, or the small scale of the indentation flaw system.

Accordingly, Figure 5 shows the results of some tests on the same indented soda lime glass system represented in Figure 4, obtained by measuring the critical applied stresses,  $\sigma_M$ , as a function of load  $P$  (24). In Figure 5a the raw data are fitted with a slope of  $-1/3$  (logarithmic coordinates), in line with Equation 23 (again using calibrated parameters  $T_0$  and  $\chi$  from the previous regressions in Figure 4 to fix the intercept). The same data are replotted in Figure 5b as  $\sigma_M P^{1/3}$  versus  $P$  to emphasize the constancy of the toughness term  $T_0$  in Equation 23. We make further use of this alternative construction in our remaining case study.

### *Microstructure-Strength Relations in Polycrystalline Alumina*

In this final example we return to polycrystalline alumina to examine the way the microstructural effects described in the section on DCB can become manifest in strength properties. Interest in this topic stems from the issue of whether crack laws determined from observations on large-scale fracture specimens can be applied to microstructural flaws. There is mounting evidence that extrapolations from the macroscale to the microscale can be extremely misleading; the strengths of materials that fail from microstructural flaws can be much less favorable than those predicted from macroscopic toughness parameters (27).

To illustrate the potential magnitude of the size effect, we show in Figure 6 some results from a recent indentation-strength study of aluminas (28) (and other ceramics). The data are plotted as  $\sigma_M$  versus  $P$  in Figure 6a and as  $\sigma_M P^{1/3}$  versus  $P$  in Figure 6b, in direct analogy to Figure 5. We are primarily interested in the polycrystalline alumina; the single crystal (sapphire) data line (28) is included solely as a reference baseline. It is immediately apparent that the polycrystal data deviate significantly from the ideal (microstructure-free) indentation-strength response defined by Equation 23. In particular, the  $\sigma_M(P)^{1/3}$  plot shows a strong increase with indentation load, thereby reflecting strong  $T$ -curve behavior.

Clearly, a complete  $\sigma_M P$  description of the polycrystal data in Figures 6a and b requires that we incorporate the microstructural stress intensity

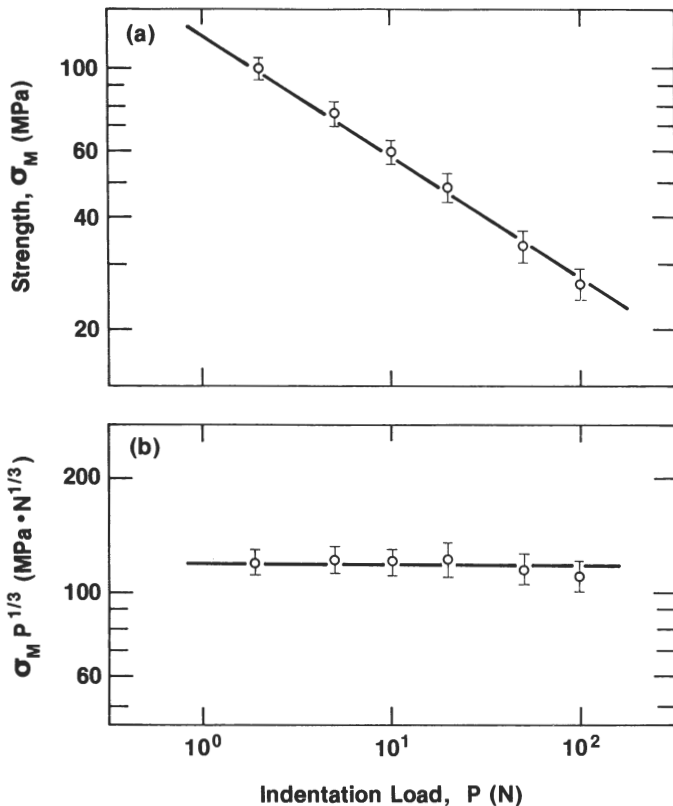


Figure 5 Inert strength data for Vickers indented glass (same material as in Figure 4): (a) direct plot as function of load; (b) replotted to confirm validity of Equation 23. (Data from Reference 23.)

factor,  $K_\mu$  in Equation 16, into the indentation analysis. This is certainly needed if we ever wish to extract the  $T$ -curve itself from the strength data. Thus we may appropriately modify the form of the equilibrium condition in Equation 10 to yield

$$K = \psi \sigma_a c^{1/2} + \chi P / c^{3/2} + K_\mu(c) = T_0, \tag{24}$$

and impose the instability requirement  $dK/dc = 0$  from Equation 11 to determine the failure states. Preliminary numerical solutions have been

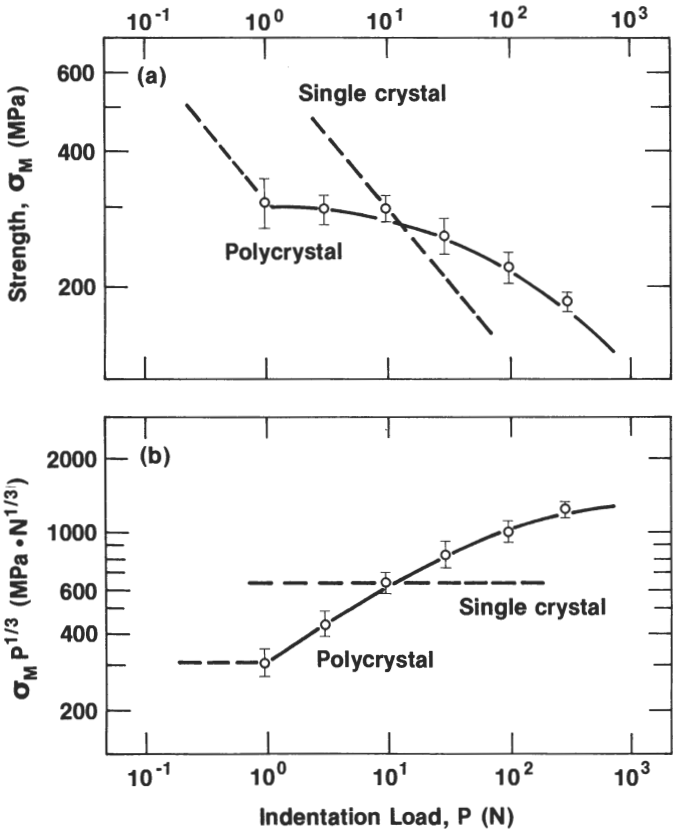


Figure 6 Inert strength data for Vickers indented polycrystalline alumina (nominally pure, grain size 25  $\mu$ m). Data for single crystal (sapphire) are included for comparison. (a) Direct plot as function of load; (b) data replotted to demonstrate breakdown of constant-toughness assumption in Equation 23. Note how the strengths of the polycrystal, although superior at high indentation loads, fall below those of the reference single crystal at low loads. In the latter region the grain boundary structure is the sole determinant of the toughness, which accounts for the cut-offs in the fitted curves. (Data from Reference 28.)

obtained elsewhere for the data in Figure 6 and were used to plot the solid curves in this figure (12). In deriving those solutions it has to be recognized that the indentation crack does not experience the microstructural restraining forces until the first ligamentary bridges are intersected, at  $c = d$  say; this accounts for the "cutoffs" in the polycrystal data at low loads in Figure 6.

The solutions to Equation 24 give us, in addition to a curve fit to the strength data in Figure 6, values for the material parameters in the  $K_{\mu}(c)$  function needed to generate the complete  $T$ -curve,  $T = T_0 - K_{\mu}$ . We plot the resultant curve for the polycrystalline alumina in Figure 7, together with the corresponding sapphire reference baseline. The  $T$ -curve shows the same general trends as those seen in Figure 1a. Any differences between the respective curves can be attributed to specimen geometry effects and to the strength of the microstructural interaction in the two polycrystalline materials. Indeed, it is found that the shape of the entire  $T$ -curve is highly sensitive to the grain boundary structure (12, 28), especially in the lower and upper bounding levels relative to the toughness of sapphire and the range of crack extension over which the curve rises.

Finally, we illustrate how complex crack stability conditions can become, especially when more than one internal  $K$ -field operates ( $K_r$  and  $K_{\mu}$ ). It has already been noted that the stabilizing influence of the microstructure does not "switch on" until  $c = d$ , whereas the corresponding stabilization due to the residual contact force operates from the inception

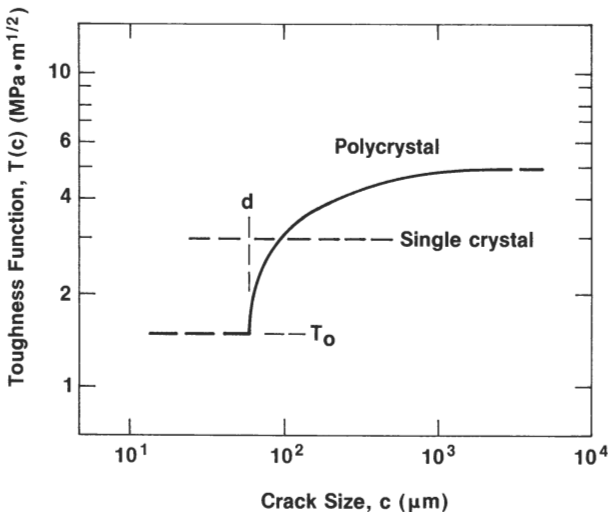


Figure 7  $T$ -curve for polycrystalline alumina, extracted from the data fits in Figure 6.

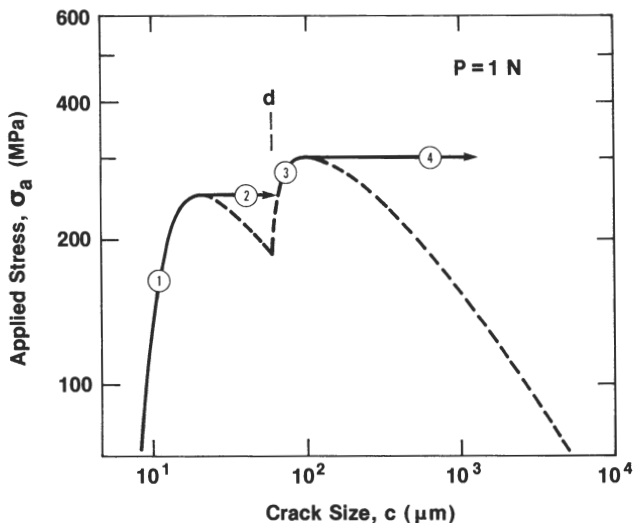


Figure 8 Applied stress versus crack size for Vickers indented alumina. Plot is for indentation flaw in a size range comparable to that of microstructural detail, using parametric evaluations from Figure 6. Note the multiple stable and unstable branches of the equilibrium curve en route to failure.

of the flaw. Hence, for low indentation loads, such that the flaw begins its life in the base region of the  $T$ -curve, we may expect some interesting crack responses as the external stress is applied. Accordingly, with the same parameter evaluations used to generate the  $T$ -curve, we compute from Equation 24 the complete  $\sigma_a(c)$  function for a selected value of  $P$  toward the extreme left of the data range in Figure 6. This function is plotted in Figure 8. The predicted sequence of events is: (1) initial stable growth, (2) unstable "pop in," (3) further stable growth, (4) unlimited instability (failure). This behavior is borne out by direct, in situ observations of indentation flaws in strength tests (12).

## SUMMARY

We have emphasized the importance of incorporating an instability requirement into the failure criteria for equilibrium brittle cracks. Our motivation has been the need to establish a proper descriptive basis for the  $T$ -curve ( $R$ -curve) phenomenology, where internal driving forces can have such a dominant influence on strength properties. The requirement for a rising  $T$ -curve is that the appropriate  $K_I(c)$  functions diminish algebraically with crack extension, i.e. either negative and increasing or

positive and decreasing. These functions are manifest as a stabilizing influence in the fracture evolution. Thus, we have seen in the indentation system that, contrary to conventional wisdom, flaws can undergo significant (sometimes multiple) stages of precursor stable growth before reaching a failure configuration. There is growing evidence that this kind of response is not restricted to artificial flaws, but is widespread in naturally occurring flaw systems as well (29).

These concerns raise strong doubts as to the validity of present-day strength analytical procedures, especially in ceramics. In particular, the time-honored notion that flaws should fail spontaneously without change in their initial configuration (the classical Griffith flaw) is at issue. Our case studies indicate that the instability configurations at failure may have little or nothing to do with the initial configurations; the precursor stable growth renders the initial flaw size irrelevant. This is illustrated most dramatically by the data for the polycrystalline alumina in Figure 6a; there is a pronounced plateau region where the strength is almost totally independent of indentation load. This has grave implications for non-destructive evaluation, for a screening test that eliminates large flaws can no longer be taken as a guarantee of a high strength.

It is, therefore, important that the  $T$ -curve be taken into account in the design of brittle materials. From the engineering standpoint, an understanding of underlying physical processes is not essential since, as we have seen, the entire  $T$ -curve can be obtained empirically. However, such an understanding is valuable in determining the extent to which the curve is material intrinsic. Specimen or component geometry, mode of loading (constant load or displacement), and crack history ("memory" of material structure) can be crucial design variables. Without a suitable physical basis for accommodating these factors in the fracture mechanics formalism, explicitly via the  $K_a(c)$  and  $K_i(c)$  functions, any extrapolation from laboratory test results to prospective service configurations is questionable.

Perhaps the most fascinating of the issues raised in this study is the relevance of the  $T$ -curve to fundamental crack laws. We prefer the single-valued parameter  $T_0$  over the function  $T(c)$  as a representative material toughness descriptor, as stated throughout our presentation.  $T_0$  conveniently quantifies the strength of the field singularity at the tip of the equilibrium crack, the region where the actual processes of material separation operate. As such, it is ultimately relatable to intrinsic surface energy terms, either for the bulk matrix or the grain boundary. The function  $T(c)$ , however, embodies the  $K_i$  terms, which depend on events that occur *away* from the crack tip (although in most of our case studies these  $K_i$  terms reflect some properties of the material). It is more meaningful to regard the  $K_i$  processes as mechanically shielding (or antishielding) the

tip from the remote applied loading (6), as implied in Equation 8. Thus it is  $K$  and not  $K_a$  that defines the true crack driving force; and it is  $K = T_0$  (Equation 10), not  $K_a = T$  (Equation 13), that comes closest to an intrinsic equilibrium material constant.

This last point can be carried over to nonequilibrium fracture, which we have not considered until now. In certain chemical environments brittle cracks grow at some rate, even in static loading tests. This rate generally increases as the applied load  $K_a$  is increased, which has led experimenters to express their data as a crack velocity function,  $v(K_a)$ . However, as we have just seen, it is the net stress intensity factor  $K$  that governs the strength of the crack-tip field, in which case it is  $v(K)$  that we derive from fundamental bond rupture kinetics (30). Hence, for cracks stabilized by closure forces ( $K_i < 0$ ) we expect slower velocities, which will be reflected as a depression of the measured  $v(K_a)$  curve (31). The potential for crack velocity shifts to manifest themselves in such interesting phenomena as "fatigue limits" (zero crack driving force,  $K = K_a + \Sigma K_i = 0$ ) remains to be explored by the brittle fracture community.

#### ACKNOWLEDGMENTS

The authors gratefully thank the following for their contributions, in the form of either discussions or original data (or both): R. F. Cook, E. R. Fuller, D. B. Marshall, M. V. Swain, and S. M. Wiederhorn. Funding was provided by the US Office of Naval Research, Metallurgy and Ceramics Program.

#### Literature Cited

- Griffith, A. A. 1920. *Philos. Trans. R. Soc. Lond. Ser. A* 221: 163-98
- Irwin, G. R. 1958. *Handbuch der Physik*, ed. S. Flügge, 6: 551-90. Springer-Verlag: Berlin
- Barenblatt, G. I. 1962. *Adv. Appl. Mech.* 7: 55-129
- Lawn, B. R., Wilshaw, T. R. 1975. *Fracture of Brittle Solids*, Chs. 1-3. London: Cambridge Univ. Press
- Broek, D. 1982. *Elementary Fracture Mechanics*, Chs. 5, 8. Boston: Martinus-Nijhoff
- Thomson, R. M. 1983. *Physical Metallurgy*, ed. R. W. Cahn, P. Haasen, pp. 1487-1551. New York: Elsevier
- Gurney, C., Mai, Y.-W. 1972. *Eng. Fract. Mech.* 4: 853-63
- Atkins, A. G., Mai, Y.-W. 1986. *Elastic and Plastic Fracture*. Chichester: Horwood/Wiley. In press
- Swain, M. V. Unpublished work
- Knechens, R., Steinbrech, R. 1982. *J. Mater. Sci. Lett.* 1: 327-29
- Fairbanks, C. J., Lawn, B. R., Cook, R. F., Mai, Y.-W. 1986. *Fracture Mechanics of Ceramics*, ed. R. C. Bradt, A. G. Evans, D. P. H. Hasselman, F. F. Lange. New York: Plenum. In press
- Mai, Y.-W., Lawn, B. R., Fairbanks, C. J., Swanson, P. L., Hockey, B. J. 1986. *J. Am. Ceram. Soc.* In press
- Heuer, A. H., Hobbs, L. W., eds. 1981. *Science and Technology of Zirconia: Advances in Ceramics*, Vol. 3. Columbus, Ohio: Am. Ceram. Soc.
- Swain, M. V., Hannink, R. H. J. 1984. *Advances in Fracture Research*, ed. S. F. Valluri, D. M. R. Taplin, P. Rama Rao, J. F. Knott, R. Dubey, pp. 2633-40. Oxford: Pergamon
- McMeeking, R. M., Evans, A. G. 1982. *J. Am. Ceram. Soc.* 65: 242-46
- Swain, M. V. 1986. *Fracture Mechanics*

- of *Ceramics*, ed. R. C. Bradt, A. G. Evans, D. P. H. Hasselman, F. F. Lange. New York: Plenum. In press
17. Marshall, D. B. 1986. *J. Am. Ceram. Soc.* In press
  18. Foote, R. M. L., Mai, Y.-W., Cotterell, B. 1980. *Advances in Cement-Matrix Composites*, ed. D. M. Roy, pp. 135-44. Pennsylvania: Mater. Res. Soc.
  19. Foote, R. M. L., Mai, Y.-W., Cotterell, B. In press
  20. Tada, H., Paris, P. C., Irwin, G. R. 1973. *A Handbook of Stress Intensity Factors*. Pennsylvania: Del Corp.
  21. Lawn, B. R., Marshall, D. B., Chantikul, P., Anstis, G. R. 1980. *J. Aust. Ceram. Soc.* 16: 4-9
  22. Lawn, B. R. 1983. *Fracture Mechanics of Ceramics*, ed. R. C. Bradt, A. G. Evans, D. P. H. Hasselman, F. F. Lange, 5: 1-25. New York: Plenum
  23. Marshall, D. B., Lawn, B. R. 1979. *J. Mater. Sci.* 14: 2001-12
  24. Marshall, D. B., Lawn, B. R., Chantikul, P. 1979. *J. Mater. Sci.* 14: 2025-35
  25. Lawn, B. R., Evans, A. G., Marshall, D. B. 1980. *J. Am. Ceram. Soc.* 63: 574-81
  26. Marshall, D. B., Lawn, B. R. 1980. *J. Am. Ceram. Soc.* 63: 532-36
  27. Pletka, B. J., Wiederhorn, S. M. 1982. *J. Mater. Sci.* 17: 1247-68
  28. Cook, R. F., Lawn, B. R., Fairbanks, C. J. 1985. *J. Am. Ceram. Soc.* 68: 604-15
  29. Lawn, B. R., Jakus, K., Gonzalez, A. C. 1985. *J. Am. Ceram. Soc.* 68: 25-34
  30. Lawn, B. R. 1975. *J. Mater. Sci.* 10: 469-80
  31. Lawn, B. R. 1985. *Appl. Phys. Lett.* 47: 809-11